Experimental Evidence of Weak Excluded Volume Effects for Nanochannel Confined DNA

Damini Gupta,[†] Jeremy J. Miller,[†] Abhiram Muralidhar,[†] Sara Mahshid,[‡] Walter Reisner,[*,‡] and Kevin D. Dorfman[*,†]

[†]Department of Chemical Engineering and Materials Science, University of Minnesota — Twin Cities, 421 Washington Avenue SE, Minneapolis, Minnesota 55455, United States

[‡]Physics Department, McGill University, 3600 rue University, Montreal QC H3A 2T8, Canada

S *Supporting Information*

ABSTRACT: We present experimental demonstration that weak excluded volume effects arise in DNA nanochannel confinement. In particular, by performing measurements of the variance in chain extension as a function of nanochannel dimension for effective channel sizes ranging from 305 to 453 nm, we show that the scaling of the variance in extension with channel size rejects the de Gennes scaling $\delta^2 X \sim D^{1/3}$ in favor of $\delta^2 X \sim D^0$ using uncertainty at the 95% confidence level. We also show how simulations and confinement spectroscopy can be combined to reduce molecular weight dispersity effects arising from shearing, photocleavage, and nonuniform staining of DNA.
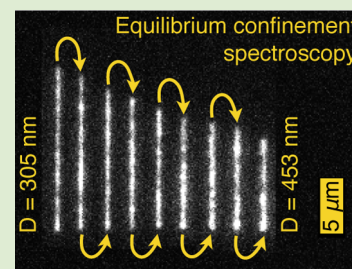
Determining the equilibrium conformation of nanochannel-confined DNA has attracted substantial attention as a fundamental problem in polymer physics[1] connected to an emerging technology for genomics.[2−7] Initially, it was proposed[8] that the de Gennes blob theory for weak confinement[9] and Odijk's deflection segment theory for strong confinement[10] provided a complete description of the thermodynamics of a semiflexible chain of persistence length l_p confined in a channel of size D. Intense simulation and theoretical efforts over the past few years[11−16] suggest that excluded volume in confinement plays a more subtle role than previously thought. In particular, in addition to the classic de Gennes blob regime, an "extended de Gennes" regime has been postulated, holding for channel sizes $l_p \lesssim D \lesssim l_p^2/w$, where w is the effective width of the polymer backbone. While both the theory of nanochannel-confined DNA[11−18] and practical applications of the technology in genomics[2−7] have advanced rapidly, the experimental evidence in support of the emerging theoretical framework is lacking. In this letter, we provide evidence in support of the weak excluded volume effects that form the physical basis for the extended de Gennes regime. In doing so, we also show how a detailed simulation combined with confinement spectroscopy can reduce molecular weight dispersity effects that are introduced into an otherwise monodisperse DNA sample due to shear,[19] photocleavage,[20,21] or heterogeneous staining.[22]

Classic de Gennes scaling theory suggests that a self-avoiding chain confined in a channel corresponds to a string of isometric blobs of diameter D (see Figure 1a).[1] Excluded-volume effects are strong, determining both the polymer physics *within* a blob (each blob is a self-avoiding coil obeying Flory statistics) and *between* blobs (self-exclusion interactions between blobs lead to their linear ordering, swelling the chain along the channel). In
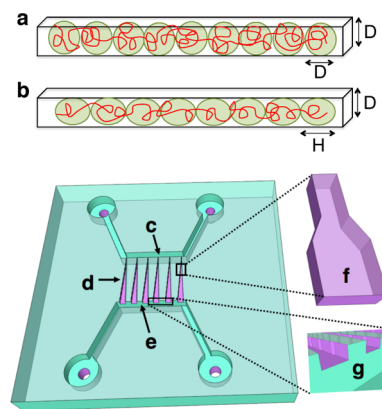

Figure 1. (a) In the classic de Gennes regime a confined self-avoiding chain corresponds to a string of isometric blobs. (b) In the extended de Gennes regime a confined and weakly self-avoiding chain corresponds to a string of anisometric blobs. (c–g) Schematic illustration of the confinement spectroscopy device. The device consists of two 1 μm deep and 50 μm wide microchannels (c,e), bridged by an array of nanofunnels (d). A single nanofunnel (f) has nine connected 300 nm deep and 45 μm long nanochannels; the width of the nanochannel varies from 350 to 750 nm in steps of 50 nm. The DNA is loaded in the nanochannel with pneumatic pressure across the intersection of the microchannel and the nanofunnel region (g). The detailed operation of this type of device is described elsewhere.[23]

contrast, the extended de Gennes regime is characterized by weak excluded volume effects.[14,15] In this regime, a chain of

persistence length l_p and width w, confined in a channel of size D, can be envisioned as a series of *anisometric* blobs[11] of diameter D and length $H \cong (Dl_p)^{2/3}w^{-1/3}$ (see Figure 1b).[17] Excluded volume between blobs leads to swelling of the chain along the channel axis, but the excluded volume interactions within a blob are marginal.[14] The swelling along the channel axis leads to a fractional extension X/L

$$X/L = 1.176(62)(l_p w/D^2)^{1/3} \qquad (1)$$

where X is the mean span of a polymer of contour length L.[12,14,15] The prefactor comes from the theory by Werner and Mehlig, which maps the extended de Gennes regime onto a one-dimensional, weakly self-avoiding walk.[15] The latter scaling is identical to that in the de Gennes regime[9] and hence the moniker "extended" de Gennes.[12] The weakness of the excluded volume interactions manifests itself in the variance in the fractional extension.[11,12,14,15,24] Since the blobs themselves are at the crossover between real and ideal chains, the variance in the fractional extension is independent of the channel size[12,14,15,24]

$$\delta^2 X/Ll_p = 0.264(99) \qquad (2)$$

where again the prefactor comes from the theory of Werner and Mehlig.[15] In contrast, in the classic de Gennes regime, $\delta^2 X \sim D^{1/3}$.[8] Note that eqs 1 and 2 are expressed in terms of the persistence length, which leads to different numerical values than the equivalent expressions in terms of Kuhn length.[15]

Demonstrating the existence of weak excluded volume effects through the scaling $\delta^2 X \sim D^0$ in the range $l_p \lesssim D \lesssim l_p^2/w$ is a key step toward establishing the existence of an extended de Gennes regime. The experimental approach seems straightforward: make a series of channels in this size range, introduce DNA into these channels, and measure the variance in the chain extension. Unfortunately, molecular weight dispersity of the DNA represents a critical obstacle to obtaining accurate measurements of the scaling exponents and, even worse, the prefactors to the scaling laws. In many cases very large DNA molecules (sometimes on the order of megabases in size) are required to reach the long chain limit.[13,25−27] While genomic DNA samples are monodisperse, such long DNA molecules are prone to shear breakage.[19] Moreover, the DNA can photo-cleave during measurements.[20] Heterogeneous staining[22] can lead to differences in L due to variations in the increased contour length as a result of intercalation between molecules. In all of these cases, the associated uncertainty in L can lead to large uncertainties in the measurement of $\delta^2 X$, thereby making the tests of the theories challenging.

We have developed an approach that combines equilibrium confinement spectroscopy[23] with Pruned-Enriched Rosenbluth Method (PERM) simulations of a confined, discrete wormlike chain[28] to reduce the effects of molecular weight dispersity. The nanochannel device, illustrated schematically in Figure 1c−g, consists of a channel of depth $D_1 = 300$ nm that cascades in discrete steps in width from $D_2 = 350$ nm to $D_2 = 750$ nm. It is thus similar to previous confinement spectroscopy devices with a continuous taper in D_2,[29] but the 45 μm long regions of constant width D_2 allow us to make measurements at equilibrium.[23] The buffer for our experiments has an ionic strength of 7.18 mM. Accounting for the effect of the antiphotobleaching agent β-mercaptoethanol at 6% v/v,[30] theory predicts a persistence length of $l_p = 69$ nm and effective width $w = 19$ nm,[23,31,32] although the accuracy of this

persistence length should be viewed in light of recent data suggesting a lower persistence length of DNA.[33]

Since our channels are rectangular, we use the effective channel width[8,12,16]

$$D_{\text{eff}} = \sqrt{(D_1 - \delta)(D_2 - \delta)} \qquad (3)$$

to map the results back to an equivalent square channel of size $D_{\text{eff}} + \delta$. The parameter δ is a wall−DNA depletion length that models the electrostatic interaction of the DNA with the walls.[1] We estimate that $\delta \approx w$.[12] Our effective channel sizes range from 305 to 453 nm, which spans much of the extended de Gennes regime; simulations by Dai et al.[14] suggest that the lower bound of the extended de Gennes regime for our conditions is 276 nm and the upper bound is 562 nm. Most of our channel sizes are also below the upper limit $D_2 = 550$ nm (assuming a prefactor of unity) where Werner and Mehlig[16] predict that the channel anisotropy will affect measurements of the variance in chain extension for our value of D_1,[23] and we check the magnitude of the anisotropy effect via simulations. Additional information about the device fabrication and buffer conditions are provided in the Supporting Information.

The key advantage of the equilibrium spectroscopy approach[23] is that the same molecule can be studied in all the channel sizes at equilibrium, making it a single-molecule study in the true sense.[34] In other words, time-domain measurements for some molecule i can be used to determine the ensemble average from an ergodic hypothesis, and repeating this measurement for different molecules provides information about the experimental uncertainty, much of which arises from a very conservative estimate of the error in the image analysis (see Supporting Information). The approach is identical to typical simulation approaches, where independent replicas (the different molecules) are used to assess the sampling errors in expectation values (the measurements from a single molecule). In our case, we first pneumatically load a T4 GT7-DNA molecule (166 kbp, Nippon Gene) from the microchannel into the $D_2 = 350$ nm region and take $n = 40$ stroboscopic measurements of the span of that molecule with a minimum sampling interval of 5 s. Let us denote the jth measurements on molecule i as $X_i^{(j)}$. The time lapse corresponds to a small value of the autocorrelation in the chain extension (see Supporting Information), which ensures that the $X_i^{(j)}$ are statistically independent. When we compute the average span for molecule i and its variance

$$X_i = (1/n) \sum_{j=1}^{n} X_i^{(j)} \qquad (4)$$

$$\delta^2 X_i = [1/(n-1)] \sum_{j=1}^{n} (X_i^{(j)} - X_i)^2 \qquad (5)$$

we assume that these values are estimates of the ensemble average, i.e., $X \approx X_i$ and $\delta^2 X \approx \delta^2 X_i$. To obtain the values of X_i and $\delta^2 X_i$ at other channel sizes, we move the same molecule successively through each value of D_2 and repeat the process. At the conclusion of this single-molecule experiment, we return the molecule to the $D_2 = 350$ nm region and image it again to confirm that the extension of the molecule has not become significantly shorter due to photocleavage or shear cleavage. We performed this single-molecule protocol with 40 molecules, of which 29 did not shorten during the long measurement period. The end result is 1160 measurements of the chain extension at

each channel size, blocked into 29 replicas for statistical averaging. The detailed criteria for rejecting fragmented molecules and additional information about the experimental protocol are provided in Supporting Information.

We found a broad distribution of extensions X_i when we binned the results in the 1 μm bins shown in Figure 2a. To see
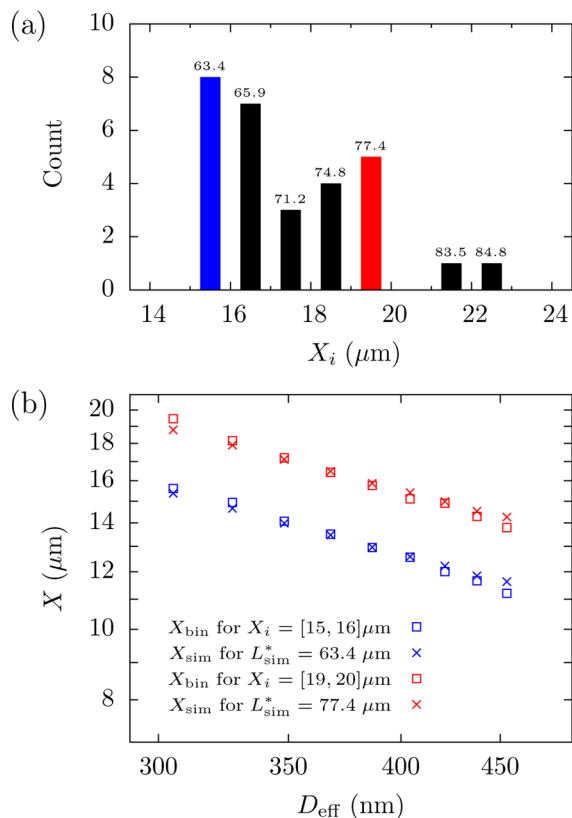

Figure 2. (a) Probability distribution of average extension, X_i, for individual T4 DNA molecules from 40 uncorrelated measurements of their span for $D_2 = 350$ nm. The bin size is 1 μm. The number above each bar is the value of the contour length in that bin, L_{bin} (μm), obtained by comparison of the extension to PERM simulations. Linear regression of L_{bin} to X_i gives a correlation coefficient $R^2 = 0.98$. (b) Log–log plot of the average value of the extension, X_{bin}, for molecules that reside in two different bins ($X_i = [15,16]$ μm in blue and $X_i = [19,20]$ μm in red) as a function of effective channel size ($\square$ symbols). To determine the corresponding molecular weight, we fit these curves to PERM simulations of the chain extension ($\times$ symbols) using the contour length as a free parameter. A plot similar to panel (b) for all of the bins is included as Supporting Information.

if this wide distribution was a result of molecular weight dispersity, we took advantage of our ability to systematically move a given molecule between different values of the channel width. To simplify our analysis, we considered how the average of the extension of the w_{bin} molecules within a given bin, $X_{bin} = (1/w_{bin}) \sum_{i=1}^{w_{bin}} X_i$, evolves as a function of D_{eff}. Figure 2b shows the results for two representative bins; the data for the other bins are included as Supporting Information. Overall, it is clear that when we bin the molecules based on their extension for $D_2 = 350$ nm, plots of X_{bin} as a function of the effective width D_{eff} are parallel curves. Since we know that $X \sim L$ for sufficiently long chains (see Supporting Information),[27] we can conclude that the distribution in Figure 2b results from molecular weight dispersity, most likely a combination of shear breakage and

nonuniform staining (which leads to nonuniform extension due to intercalation).[22]

To compute the nominal contour length L_{bin} for those molecules in a given bin of Figure 2a, we performed PERM simulations of a discrete wormlike chain in a rectangular channel for each value of D_2. These simulations follow directly from our prior work,[23] and a brief description is provided in the Supporting Information. Importantly, PERM provides data for the simulated extension, X_{sim}, in a given rectangular channel size as a function of simulated contour length, L_{sim}. For each channel, we ran our simulations out to approximately double the contour length of unstained T4 DNA, well beyond any possible effect due to intercalation.[35,36] Then, for each bin in Figure 2a, we determined the value of L_{sim}^* that minimized the sum of squared error in $X_{sim} - X_{bin}$ over all the channel sizes and set $L_{bin} = L_{sim}^*$. Figure 2b reports the result of this analysis for two bins, and the corresponding analysis for the other bins is included as Supporting Information. The data in Figure 2b indicate that there is some disagreement between the simulation and experimental data. However, the L_{bin} values are linearly dependent on X_i to within 2% error. There may also be a systematic error in L_{bin}, but this will only affect the prefactor and not the exponent in the scaling law (see Supporting Information).

The ultimate result of our binning-and-simulation protocol is estimates for the contour length of molecules within each bin, which are reported in Figure 2a. In what follows, we use the value of L_{bin} as the contour length L_i for any molecule within that bin, thereby compensating for the effects of molecular weight dispersity by rescaling each molecule by its L_i value. We are now in a position to determine the validity of eq 2 for the variance in chain extension, which is the key prediction arising from weak excluded volume effects in the extended de Gennes regime.

The independence of the variance in extension from channel size in Figure 3 demonstrates that weak excluded volume effects are manifest for DNA in nanochannel confinement. This is the
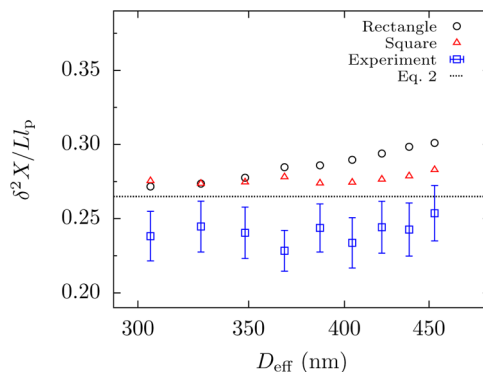

Figure 3. Semilog plot of the average variance in extension, $\delta^2 X$, as a function of effective channel size, D_{eff}, for rectangular channels with depth $D_1 = 300$ nm and widths D_2 ranging from 350 to 750 nm. The experimental mean extension variance (blue $\square$) are the mean of 29 molecules. Error bars represent the combination of standard error of the mean and propagation of measurement uncertainty (see Supporting Information). PERM simulations in the rectangular channels of dimension $D_1 = 300$ nm and $D_2 = 350$ to 750 nm for a contour length $L = 70.2$ μm are included for rectangular channels (black $\bigcirc$) and equivalent square channels (red $\triangle$) of size $D_{eff} + w$. Error bars for the simulation data are smaller than the symbol size. The black dashed line is eq 2.

key result of this letter. We find experimentally that the variance in chain extension has the scaling $\delta^2 X/Ll_p \sim D_{eff}^{0.08\pm0.18}$, where the uncertainty in the exponent is at the 95% confidence level. We also did an alternate analysis, where we obtained the exponent for each molecule and then computed their average. This led to $\delta^2 X/Ll_p \sim D_{eff}^{0.05\pm0.27}$ at the same confidence. Note that this alternate method provides the exponent but no information about the prefactor since it does not require estimating L or l_p. A hypothesis test at the 5% significance level rejects the $\delta^2 X/Ll_p \sim D_{eff}^{1/3}$ hypothesis in favor of the $\delta^2 X/Ll_p \sim D_{eff}^0$ hypothesis by both analysis methods. Our variance data agree to within 8% of the theoretical prefactor predicted by Werner and Mehlig and to within 16% of the PERM data. However, while we believe the agreement for the scaling exponent is robust to our data analysis method, the agreement for the prefactor must be viewed in light of the method to determine L_{bin}. A discussion of this subtle point is included in the Supporting Information. Moreover, the error estimates in Figure 3 do not include uncertainties in L or l_p. These sources of correlated error affect the prefactor but do not affect the slope. Thus, it seems reasonable to conclude that the agreement for the prefactor is semiquantitative.

We also checked for anisotropy effects due to the rectangular shape of the channel[16,23] by performing PERM simulations in square channels with size $D_{eff} + w$. Figure 3 shows no systematic deviation in the simulated values of $\delta^2 X/Ll_p$ between square channels and rectangles up to the aspect ratio $D_2/D_1 = 1.7$ of the widest rectangular channel. There does appear to be a small difference for $D_{eff} > 370$ nm. However, the maximum difference between the rectangular channels and the equivalent square channel was close to 6%, which is of the same order of magnitude as the uncertainty in the experimental measurement. We thus conclude that any anisotropy effect in these experiments is much smaller than the ca. 200% increase that occurs in the 100 nm deep rectangular channels that exhibit regime mixing.[23]

While the simulations in square channels produce an exponent similar to the experiments ($\delta^2 X/Ll_p \sim D_{eff}^{0.05\pm0.05}$ at 95% confidence), the simulations for the rectangular channels reject both classical and extended de Gennes regime hypothesis at the 5% significance level ($\delta^2 X/Ll_p \sim D_{eff}^{0.27\pm0.03}$). The discrepancy between simulation and experiments likely arises from the uncertainty in the estimation of parameters which goes into the model used for PERM simulations. We will revisit this uncertainty later in our discussion of the extension results.

Figure 4 summarizes the different results for the average fractional extension of the chain, X/L, as a function of effective channel size, D_{eff}. The relatively good quantitative agreement between the PERM simulations and experimental data results from using L as a fitting parameter, whereupon the only significant metric for comparison is the power law exponent.[23] The experimental data produce a scaling of $X \sim D_{eff}^\alpha$ with $\alpha = -0.86 \pm 0.02$. Similar to many previous studies of nanochannel confined DNA,[8,29,37] we find that the apparent exponent is more negative than the predictions from weakly self-avoiding random walk theory ($\alpha = -2/3$, eq 1),[15] predictions based on a corrected Flory exponent[12,14] ($\alpha = -0.7015$), or our simulations in rectangular channels ($\alpha = -0.71 \pm 0.01$).

Disagreement between theory and simulation results in Figure 4 likely arises from the finite molecular weight. As shown in Supporting Information, PERM simulations for our rectangular channels suggest that the magnitude of the apparent exponent α slowly declines with molecular weight once the
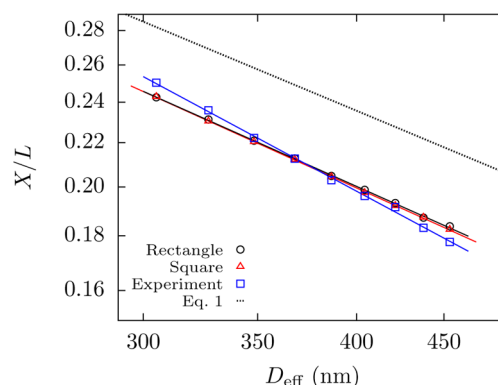

Figure 4. Log−log plot of the average fractional extension, X/L, as a function of effective channel size, D_{eff}. The experimental data (blue □) are the average of 29 molecules. Power law fit to the data yields an exponent $\alpha = -0.86 \pm 0.03$. The uncertainty in the exponent is determined from a combination of propagation of 95% confidence interval for the exponent of an individual molecule and its standard error of the mean. PERM simulations in the rectangular channels (black ○) and square channels (red △) were calculated for $L = 70.2$ μm. Power law fit to the data yields an exponent $\alpha = -0.71 \pm 0.01$ for the rectangular channel and $\alpha = -0.72 \pm 0.01$ for the square channel. The uncertainties in the exponent for the simulations are determined from 95% confidence intervals. The error bars for the extension are smaller than the symbol size. The black dashed line is eq 1.[15] The prefactor for the simulated extension is similar to previous work.[14,24]

chain is large enough to form several blobs, only reaching the asymptotic value for the experimentally impractical scenario of DNA in the megabase range. Disagreement between simulation and experimental data in Figures 3 and 4 likely arises from uncertainties on the precise value of the persistence length at our salt concentration,[33] possible changes in ionic strength during the experiment, and the exact value of the wall depletion length δ. We feel in particular that errors arising from the depletion length might explain the steeper dependence of the experimental extension on channel size compared with simulation. The variance data, independent of channel size, should be affected only by errors on the persistence length, explaining why the variance data agree better with simulation than the extension. We also see quantitative disagreement between eq 1 and our experiments and simulations, as was the case with previous simulations.[14]

In summary, we have provided experimental evidence supporting the theoretical prediction of weak excluded volume in the extended de Gennes regime. Simultaneously, we developed an approach to account for the effect of molecular weight dispersity effects. These experiments represent the first test of the emerging theoretical framework describing channel-confined DNA.[11] The complete experimental test of the phase diagram for channel-confined DNA, with careful control over molecular weight dispersity, will provide a firm foundation for the emerging genomic technology.[2−7]

■ ASSOCIATED CONTENT

Ⓢ Supporting Information

Experimental methods, evaluation of quantitative agreement with theory, and simulation methodology. The Supporting Information is available free of charge on the ACS Publications website at DOI: 10.1021/acsmacrolett.5b00340.

AUTHOR INFORMATION

Corresponding Authors
*E-mail: reisner@physics.mcgill.ca.
*E-mail: dorfman@umn.edu.

Notes
The authors declare no competing financial interest.

REFERENCES

(1) Reisner, W.; Pedersen, J. N.; Austin, R. H. *Rep. Prog. Phys.* **2012**, *75*, 106601.
(2) Persson, F.; Tegenfeldt, J. O. *Chem. Soc. Rev.* **2010**, *39*, 985−999.
(3) Lam, E. T.; Hastie, A.; Lin, C.; Ehrlich, D.; Das, S. K.; Austin, M. D.; Deshpande, P.; Cao, H.; Nagarajan, N.; Xiao, M.; Kwok, P.-Y. *Nat. Biotechnol.* **2012**, *30*, 771−776.
(4) Welch, R. L.; Sladek, R.; Dewar, K.; Reisner, W. W. *Lab Chip* **2012**, *12*, 3314−3321.
(5) Hastie, A. R.; Dong, L.; Smith, A.; Finkelstein, F.; Lam, E. T.; Huo, N.; Cao, H.; Kwok, P.-Y.; Deal, K. R.; Dvorak, J.; Luo, M.-C.; Gu, Y.; Xiao, M. *PLoS One* **2013**, *8*, e55864.
(6) Cao, H.; et al. *GigaScience* **2014**, *3*, 34.
(7) Nilsson, A. N.; Emilsson, G.; Nyberg, L. K.; Noble, C.; Stadler, L. S.; Fritzsche, J.; Moore, E. R.; Tegenfeldt, J. O.; Ambjörnsson, T.; Westerlund, F. *Nucleic Acids Res.* **2014**, *42*, e118.
(8) Reisner, W.; Morton, K. J.; Riehn, R.; Wang, Y. M.; Yu, Z.; Rosen, M.; Sturm, J. C.; Chou, S. Y.; Frey, E.; Austin, R. H. *Phys. Rev. Lett.* **2005**, *94*, 196101.
(9) Daoud, M.; de Gennes, P.-G. *J. Phys. (Paris)* **1977**, *38*, 85−93.
(10) Odijk, T. *Macromolecules* **1983**, *16*, 1340−1344.
(11) Odijk, T. *Phys. Rev. E* **2008**, *77*, 060901(R).
(12) Wang, Y.; Tree, D. R.; Dorfman, K. D. *Macromolecules* **2011**, *44*, 6594−6604.
(13) Dai, L.; Tree, D. R.; van der Maarel, J. R. C.; Dorfman, K. D.; Doyle, P. S. *Phys. Rev. Lett.* **2013**, *110*, 168105.
(14) Dai, L.; van der Maarel, J.; Doyle, P. S. *Macromolecules* **2014**, *47*, 2445−2450.
(15) Werner, E.; Mehlig, B. *Phys. Rev. E* **2014**, *90*, 062602.
(16) Werner, E.; Mehlig, B. *Phys. Rev. E* **2015**, *91*, 050601(R).
(17) Brochardt-Wyart, F.; Tanaka, T.; Borghi, N.; de Gennes, P.-G. *Langmuir* **2005**, *21*, 4144−4148.
(18) Muralidhar, A.; Tree, D. R.; Dorfman, K. D. *Macromolecules* **2014**, *47*, 8446−8458.
(19) Kovacic, R. T.; Comai, L.; Bendich, A. J. *Nucleic Acids Res.* **1995**, *23*, 3999−4000.
(20) Akerman, B.; Tuite, E. *Nucleic Acids Res.* **1996**, *24*, 1080−1090.
(21) Alizadehheidari, M.; Werner, E.; Noble, C.; Reiter-Schad, M.; Nyberg, L.; Fritzsche, J.; Mehlig, B.; Tegenfeldt, J. O.; Abjornsson, T.; Persson, F.; Westerlund, F. *Macromolecules* **2015**, *48*, 871−878.
(22) Nyberg, L.; Persson, F.; Åkerman, B.; Westerlund, F. *Nucleic Acids Res.* **2013**, *41*, e184.
(23) Gupta, D.; Sheats, J.; Muralidhar, A.; Miller, J. J.; Huang, D. E.; Mahshid, S.; Dorfman, K. D.; Reisner, W. *J. Chem. Phys.* **2014**, *140*, 214901.
(24) Dai, L.; Doyle, P. S. *Macromolecules* **2013**, *46*, 6336−6344.
(25) Tree, D. R.; Muralidhar, A.; Doyle, P. S.; Dorfman, K. D. *Macromolecules* **2013**, *46*, 8369−8382.
(26) Mansfield, M. L.; Douglas, J. F. *Soft Matter* **2013**, *9*, 8914−8922.
(27) Muralidhar, A.; Tree, D. R.; Wang, Y.; Dorfman, K. D. *J. Chem. Phys.* **2014**, *140*, 084905.
(28) Tree, D. R.; Wang, Y.; Dorfman, K. D. *Phys. Rev. Lett.* **2013**, *110*, 208103.
(29) Persson, F.; Utko, P.; Reisner, W.; Larsen, N. B.; Kristensen, A. *Nano Lett.* **2009**, *9*, 1382−1385.
(30) Hsieh, C.-C.; Balducci, A.; Doyle, P. S. *Nano Lett.* **2008**, *8*, 1683−1688.
(31) Stigter, D. *Biopolymers* **1977**, *16*, 1435−1448.
(32) Dobrynin, A. V. *Macromolecules* **2006**, *39*, 9519−9527.
(33) Brunet, A.; Tardin, C.; Salomé, L.; Rousseau, P.; Destainville, N.; Manghi, M. *Macromolecules* **2015**, *48*, 3641−3652.
(34) Frykholm, K.; Alizadehheidari, M.; Fritzsche, J.; Wigenius, J.; Modesti, M.; Persson, F.; Westerlund, F. *Small* **2014**, *10*, 884−887.
(35) Bakajin, O. B.; Duke, T. A. J.; Chou, C. F.; Chan, S. S.; Austin, R. H.; Cox, E. C. *Phys. Rev. Lett.* **1998**, *80*, 2737−2740.
(36) Randall, G. C.; Doyle, P. S. *Macromolecules* **2005**, *38*, 2410−2418.
(37) Werner, E.; Persson, F.; Westerlund, F.; Tegenfeldt, J. O.; Mehlig, B. *Phys. Rev. E* **2012**, *86*, 041802.
(38) Iarko, V.; Werner, E.; Nyberg, L.; Müller, V.; Fritzsche, J.; Ambjörnsson, T.; Beech, J. P.; Tegenfeldt, J. O.; Mehlig, K.; Westerlund, F.; Mehlig, B. *arXiv* **2015**, 1506.02241.

NOTE ADDED IN PROOF

A preprint[38] comparing the extended de Gennes theory and experimental data appeared online after the submission of this letter.